Ocean Sci., 12, 137–151, 2016
www.ocean-sci.net/12/137/2016/
doi:10.5194/os-12-137-2016

Ocean Science Open Access EGU

Temporal evolution of the momentum balance terms and frictional adjustment observed over the inner shelf during a storm

M. Grifoll[1,2], **A. L. Aretxabaleta**[3], **J. L. Pelegrí**[4], **and M. Espino**[1,2]

[1]Technical University of Catalonia, Barcelona, Spain
[2]International Centre of Coastal Resources Research, Barcelona, Spain
[3]US Geological Survey, Woods Hole, MA, USA
[4]Departament d'Oceanografia Física i Tecnològica, Institut de Ciències del Mar, CSIC, Barcelona, Spain

Correspondence to: M. Grifoll (manel.grifoll@upc.edu)

Received: 27 April 2015 – Published in Ocean Sci. Discuss.: 27 May 2015
Revised: 16 December 2015 – Accepted: 21 December 2015 – Published: 18 January 2016

Abstract. We investigate the rapidly changing equilibrium between the momentum sources and sinks during the passage of a single two-peak storm over the Catalan inner shelf (NW Mediterranean Sea). Velocity measurements at 24 m water depth are taken as representative of the inner shelf, and the cross-shelf variability is explored with measurements at 50 m water depth. During both wind pulses, the flow accelerated at 24 m until shortly after the wind maxima, when the bottom stress was able to compensate for the wind stress. Concurrently, the sea level also responded, with the pressure-gradient force opposing the wind stress. Before, during and after the second wind pulse, there were velocity fluctuations with both super- and sub-inertial periods likely associated with transient coastal waves. Throughout the storm, the Coriolis force and wave radiation stresses were relatively unimportant in the along-shelf momentum balance. The frictional adjustment timescale was around 10 h, consistent with the *e*-folding time obtained from bottom drag parameterizations. The momentum evolution at 50 m showed a larger influence of the Coriolis force at the expense of a decreased frictional relevance, typical in the transition from the inner to the mid-shelf.

1 Introduction

The inner shelf, encompassing depths ranging from a few to tens of meters, is dynamically defined as the region that lies between the surf zone (where waves break and the momentum balance is dominated by wave-induced terms) and the mid-shelf (where the along-shelf circulation is usually in geostrophic balance) (Lentz and Fewings, 2012). The circulation over the inner shelf is often investigated through the analysis of the momentum balance in different regions, although most studies have usually focused on those conditions averaged over periods longer than 1 week (Lee et al., 1984; Lentz and Winant, 1986; Lentz et al., 1999, Maza et al., 2006; Fewings and Lentz, 2010; Grifoll et al., 2012, 2013). In contrast, the analysis of the momentum terms at daily and shorter timescales under rapidly changing forcing conditions remains less explored.

Energetic wind events, such as storms, modify the typical pattern of water circulation over the continental shelf. The proximity of the coastline and the relevance of bottom friction prevent the generation of inertial fluctuations, which often prevail in the mid- and outer-shelf following wind pulses (Salat et al., 1992; Shearman, 2005). Additionally, during the passage of storms, the intense wind, and in some cases the associated cooling, affects a large fraction of the water column. The frictional adjustment time, proportional to water depth and inversely proportional to wind stress, is largely reduced nearshore during such energetic events. As a consequence, the magnitude, phase and relative importance of the dominant terms in the momentum balance is modified. For instance, during the passage of the tropical storm Floyd along the US east coast, Kohut et al. (2006) found an increase in both wind stress and the horizontal pressure gradient, with a change in the sign of the terms between the storm and the subsequent relaxation period. During winter wind events on the US east coast, Lee et al. (1984) found evidence of the

sea-level slope opposing the wind stress in order to establish a frictional equilibrium that differed from the average conditions. A seasonal study of the Catalan shelf (Grifoll et al., 2013) suggested that the occurrence of one single intense event can dominate the monthly averaged momentum balance, with water piling against the coast as a response to the enhanced wind stress; to balance the surface forcing, the bottom stress term was also increased.

In this paper, we investigate the temporal evolution of the momentum balance terms over relatively short timescales (of order 1 day) during the passage of a storm. The analysis is based on a set of observations from the Catalan inner shelf (offshore the city of Barcelona, NW Mediterranean Sea; Fig. 1). The prevalent momentum terms at two different depths (24 and 50 m) are examined. We take advantage of our setting in a micro-tidal environment to investigate a temporal scale (from hours to a few days) usually not considered in the literature, where the time series are often low-pass filtered to remove the short-term fluctuations (e.g., tidal flow). The goal is to quantify the different momentum terms during the storm and to examine the response timescales of the inner-shelf environment to the principal forcing mechanisms.

2 Site location, data and methods

The Catalan shelf is micro-tidal, with tidal amplitudes of the order of 0.1 m. The wind and heat flux regimes exhibit a seasonal cycle associated with the Mediterranean climate and the periodicity of meteorological events in the region. Wind intensity usually has a minimum during summer and is more energetic during fall, winter and spring. During these last seasons, regional storms are predominantly associated with north and northeast winds alternating with northwesterly wind pulses (land winds). Grifoll et al. (2013) analyzed the resulting seasonal circulation pattern over the inner shelf through a combination of numerical and observational techniques. The flow is prevalent in the along-shelf direction year-round, which is consistent with the coastal constraint and the shallowness of the area. The monthly averaged along-shelf momentum balance was between wind stress and pressure gradient, with bottom stress being a second-order term.

In the present study, we focus on a subset of the data analyzed by Grifoll et al. (2012) that includes an energetic event lasting a few days during March 2011. The bulk of the measurements correspond to a field experiment conducted over the Catalan inner shelf in the framework of the FIELD_AC project (Grifoll et al., 2012). The data set consisted of velocity time series from three Acoustic Doppler Current Profiler (ADCP) deployments, each with a pressure sensor (A1 [AWAC], A2 [AWAC] and A3 [RDI]; Fig. 1). The ADCP bin size was 1 m for A1 and A2, and 2 m for A3 station; the velocity accuracy was $\pm 0.5\,\mathrm{cm\,s^{-1}}$. The along-shelf distance between A1 and A2 was 4 km. A1 and A2 were deployed less than 1 km from the coast (24 m bottom depth) while A3 was 3 km away from the coast (50 m bottom depth). Wind data were collected using a mast located at a Coastal Station Observatory (CSO; www.pontdelpetroli.org; see Fig. 1). In addition, 43 conductivity-temperature-depth (CTD) profiles were collected between 17 March and 10 April 2011 in the area surrounding the ADCPs (Grifoll et al., 2012, described the temperature and salinity conditions). Additionally, synoptic information for the storm (winds and sea-level pressure) was obtained from the ERA-Interim global reanalysis product by the European Centre for Medium Range Weather Forecasting (ECMWF).

Wave data were recorded through a directional wave buoy [Datawell DWR-G7] moored at A3. A numerical wave model SWAN (Booij et al., 1999) was implemented and calibrated for a region that covers our study area, providing the wave variables with 50 m resolution to estimate the wave-induced momentum terms. The numerical domain is shown in Fig. 1 and the implementation details were presented in Grifoll et al. (2014).

The time series used for estimating the momentum terms have been low-pass filtered with a $1/12\,\mathrm{h^{-1}}$ cutoff frequency to avoid short time fluctuations. This choice of filter window is a compromise that allows for capturing momentum changes in timescales as short as 6 h and still removing short fluctuations, from minutes to a few hours. It is also consistent with observations of low energy at frequencies much higher than inertial (Grifoll et al., 2012).

3 Results

3.1 Event description

The currents during the entire March–April 2011 field campaign were analyzed in a previous study (Grifoll et al., 2012), highlighting the prevalence of the along-shelf direction and the high correlation between the velocities measured at A1, A2 and A3. For this reason, we focus on the A2 observations, considered to be representative of the dynamics in the inner shelf, and use A1 and A3 to support the momentum-term estimates. The investigation of the cross-shelf variability in the along-shelf momentum equation also uses A3.

We focus on the 12–15 March 2011 period, which includes the passing of a NE storm with maximum wind velocity of $13\,\mathrm{m\,s^{-1}}$. The storm arose from the detachment of a low-pressure center from the jet stream between 11 and 12 March 2011, which reached the Iberian Peninsula (Fig. 2). The low pressure remained centered over the Iberian Peninsula on 13 and 14 March, and by 15 March it weakened considerably. In our region, it was characterized by two energetic northeasterly wind peaks of similar magnitude (12 March 05:00 UTC and 14 March 15:00 UTC). A relatively calm period in between the peaks lasted 22 h, with a slight reverse in wind direction (Fig. 3a), caused by the location of the low-

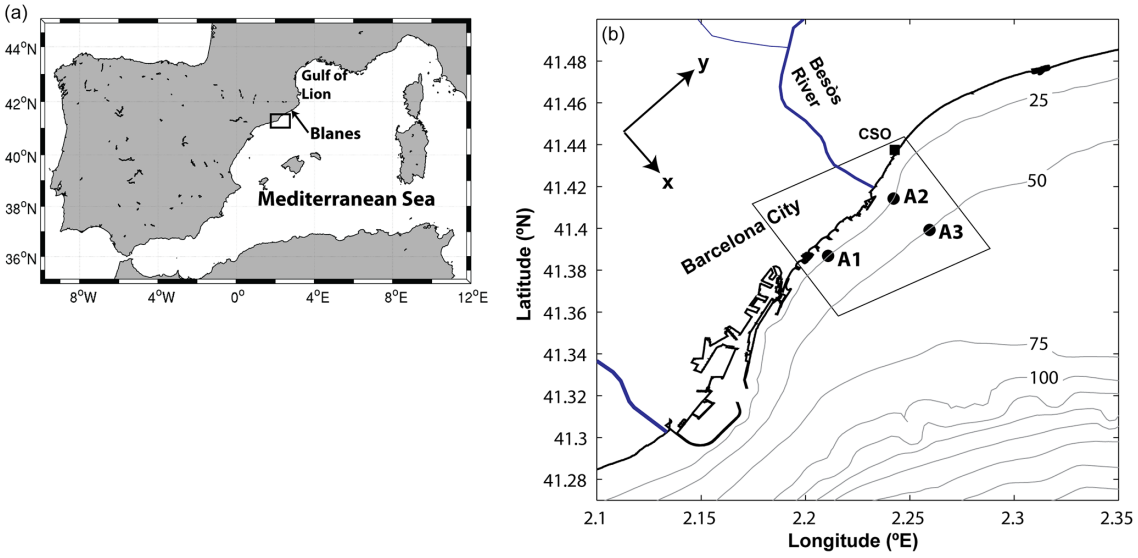

Figure 1. Map of the western Mediterranean Sea with the study area **(a)**. **(b)** Shows the bathymetry of a portion of the Catalan shelf (isobaths every 25 m) with the locations of the ADCP sensors (A1, A2 and A3). A directional wave buoy was placed at A3. The square marker shows the Coastal Station Observatory (CSO) where the wind data were recorded. **(b)** Includes the numerical model domain used to propagate the wave conditions into A2 (black rectangle); the reference system adopted for the momentum balance is also shown.

pressure center over the study area. The storm finished on 15 March when the wind intensity decreased to zero.

The along-shelf velocity (Fig. 3b) was characterized by a prevalent southwestward flow in the entire water column, with near-surface velocities typically 4 times larger than the near-bottom flow. The cross-shelf flow (Fig. 3c) was less intense than the along-shelf flow and exhibited a complex vertical structure. As a result, the depth-averaged along-shelf velocities were much larger than the depth-averaged cross-shelf velocities during the two wind peaks (Fig. 3d), reflecting a strong flow polarization associated with the coastal constraint.

During the first day of the storm (12 March), the depth-averaged along-shelf current (Fig. 3d) was toward the southwest with a maximum at 07:00 UTC (2 hours after the wind stress peak). During the calm day (13 March 00:00–22:00 UTC), the wind changed direction slightly toward the northeast (peaking at 15:00 UTC), but the along-shelf currents maintained a similar magnitude and structure than the day before. During the second wind peak the situation repeated itself, but with the along-shelf flow displaying some oscillations. The wind measurements are in good agreement with the values expected from the synoptic charts in Fig. 2.

The cross-shelf currents also displayed a similar time evolution during both wind peaks: the cross-shelf flow intensified with the wind, onshore at the surface and offshore near the bottom; as the wind stress decreased, the flow reversed, turning offshore at the surface and onshore near the bottom (Fig. 3d). During the calm day, the cross-shelf flow was weakly onshore. Following the second wind peak (14 March 16:00 UTC), the surface wind stress decreased gradually from 0.2 Pa to zero (15 March 23:00 UTC). The along-shelf flow remained to the southwest throughout the water column, and the cross-shelf flow was offshore in the sub-surface layers balanced by onshore currents near bottom.

The detided sea level (Fig. 3e) increased during both wind peaks and slowly decreased after the last wind peak. After the storm, the sea level increased as a result of water being piled up against the coast due to the northeasterly wind. The wave conditions measured at A3 were characterized by two significant wave height peaks (Fig. 3f) from the E–SE direction with 8 s period. The peaks of significant wave height followed the peaks of (along-shelf) wind stress, with a delay longer than for the along-shelf currents because of the influence of swell.

3.2 Momentum balance in the inner shelf

Assuming hydrostatic balance, ignoring the sea-level variations as compared with the total water depth, and neglecting the baroclinic terms (estimated as small in Grifoll et al., 2012, 2013), the depth-averaged along-shelf momentum balance equation can be written as

$$\underbrace{\frac{\partial \bar{v}}{\partial t}}_{\text{ACCE.}} + \underbrace{\frac{\partial \bar{v}\bar{v}}{\partial y} + \frac{\partial \bar{u}\bar{v}}{\partial x}}_{\text{ADVEC.}} + \underbrace{\frac{\bar{v}\bar{v}}{H}\frac{\partial H}{\partial y} + \frac{\bar{u}\bar{v}}{H}\frac{\partial H}{\partial x}}_{\text{CROS.SLP.}} + \underbrace{f\bar{u}}_{\text{COR.}}$$
$$= \underbrace{-g\frac{\partial n}{\partial y}}_{\text{PRS.GRD.}} + \underbrace{\frac{\tau_{ys}}{\rho H}}_{\text{W.STR.}} - \underbrace{\frac{\tau_{yb}}{\rho H}}_{\text{B.STR.}} - \underbrace{\frac{1}{\rho H}\left(\frac{\partial S_{yy}}{\partial y} + \frac{\partial S_{xy}}{\partial x}\right)}_{\text{RAD.STR.}}, \quad (1)$$

where $(\bar{u},\bar{v})$ are the cross- (x) and along-shelf (y) depth-averaged components of velocity, H is the water depth, f is

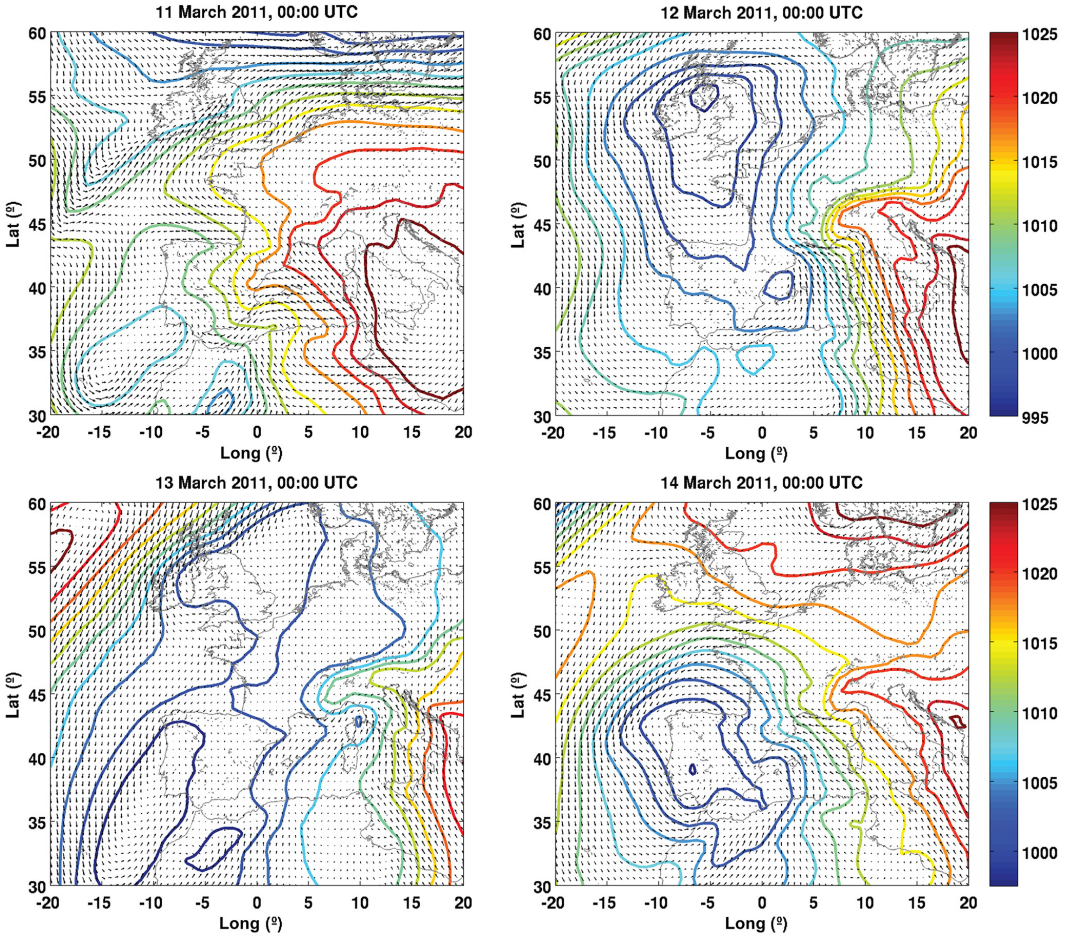

Figure 2. Regional charts of the mean sea-level pressure (HPa) and winds for the sequence 11–14 March 2011. Data source: ERA-Interim global reanalysis from ECMWF.

the Coriolis parameter ($f = 9.6 \times 10^{-5}\,\mathrm{s}^{-1}$), ρ is the water density ($1025\,\mathrm{kg\,m}^{-3}$), η is the sea-level perturbation associated with the barotropic component of the flow, τ_{ys} is the along-shelf wind stress, τ_{yb} is the along-shelf bottom stress and S_{yy}, S_{xy} represent the wave-induced mass fluxes estimated via radiation stresses (Longuet-Higgins and Stewart, 1964).

The along-shelf acceleration term at A2 (ACCE. in Eq. 1) is estimated from the observations using finite-centered differences with the velocity recorded at A2 (Fig. 4a). A negative peak is observed in the acceleration time series during the first wind peak. During 13 March, about 1 day after the first wind peak and shortly after the wind weakened (and even reversed), the acceleration term displayed an oscillatory pattern with a repeat interval of about 1 day or less.

The non-linear or advective terms are estimated by finite differentiation between the adjacent ADCP measurements (Kirincich and Barth, 2009; Fig. 4b). The velocity advection terms (ADVEC. in Eq. 1) were small during the first peak of the storm but later oscillated in a manner similar to the acceleration term. There are two additional momentum advection terms related to changes in the depth of the water column: $\left(\frac{\bar{u}\bar{v}}{H}\right)\frac{\partial H}{\partial x} + \left(\frac{\bar{v}\bar{v}}{H}\right)\frac{\partial H}{\partial y}$. The first term, the cross-shelf slope term (CROS.SLP.), has to be retained in our analysis, while the second term is zero, as the water depth is constant in the along-shelf direction.

The Coriolis term (COR in Eq. 1), computed from the depth-averaged cross-shelf velocities at A2, is small in comparison with the acceleration term during the storm (Fig. 4c). Although the surface and sub-surface cross-shelf flows were relatively important through the water column (Fig. 3c), the depth-averaged cross-shelf flow was much smaller than the along-shelf velocities (Fig. 3d). The size of this term was 4 times smaller than the acceleration term.

The along-shelf wind stress term (W.STR. in Eq. 1; Fig. 4d) was calculated using a neutral drag law (Large and Pond, 1981) from winds measured at the nearby meteorological station (Fig. 1). There was a good correspondence between wind stress and along-shelf velocity (Fig. 3a and d). The maximum (negative) acceleration, however, occurred a

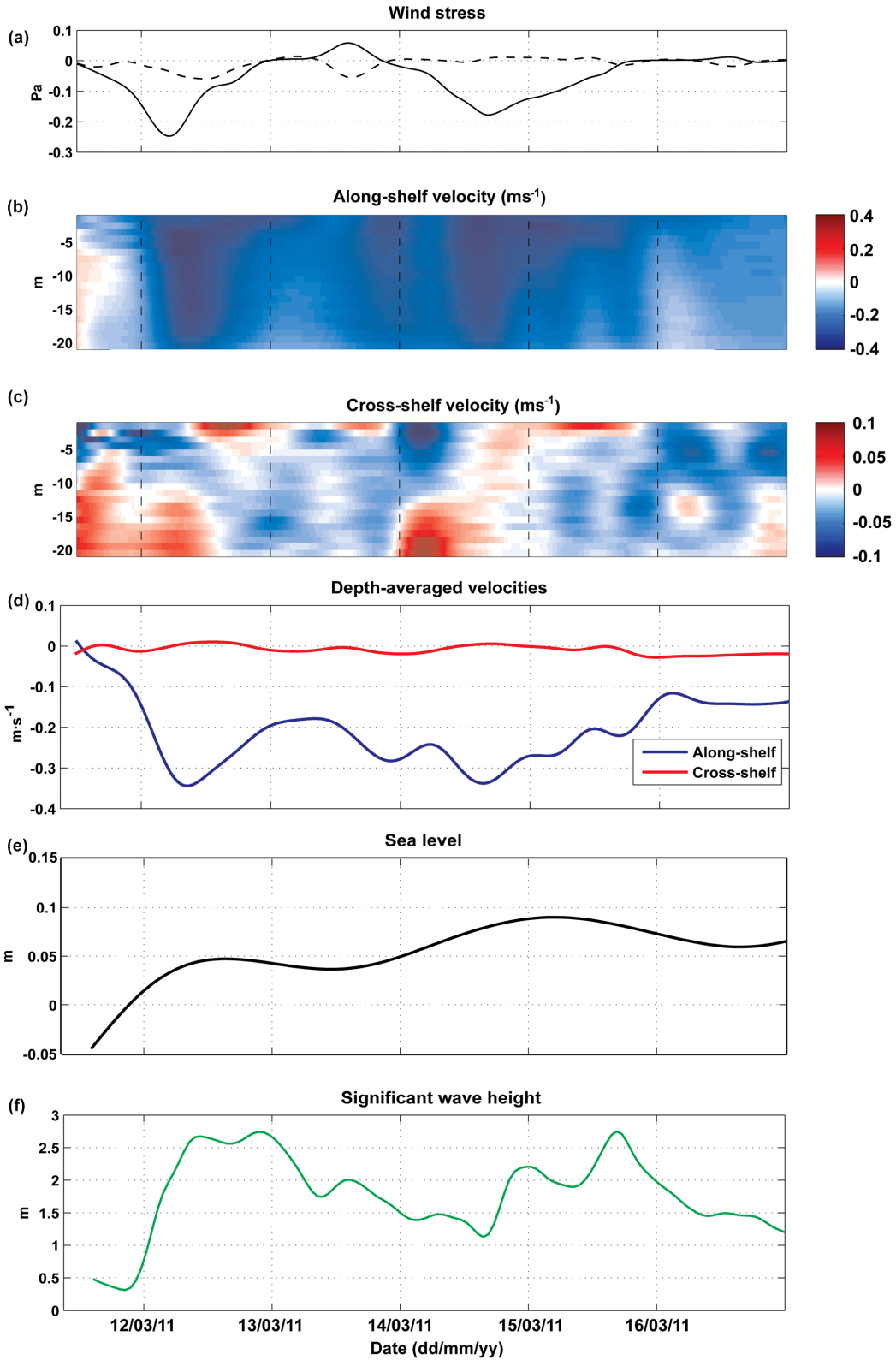

Figure 3. (a) Time series of wind stress measured at the CSO (the continuous line for the along-shelf wind component and the dashed line for the cross-shelf wind component). **(b)** Along-shelf velocity. **(c)** Cross-shelf velocity. **(d)** Depth-averaged along- and cross-shelf velocities. **(e)** Detided sea-level variations. **(f)** Significant wave-height. The velocities and sea-level fluctuations were measured at station A2, and the wave conditions at station A3. The date indicates 00:00 UTC.

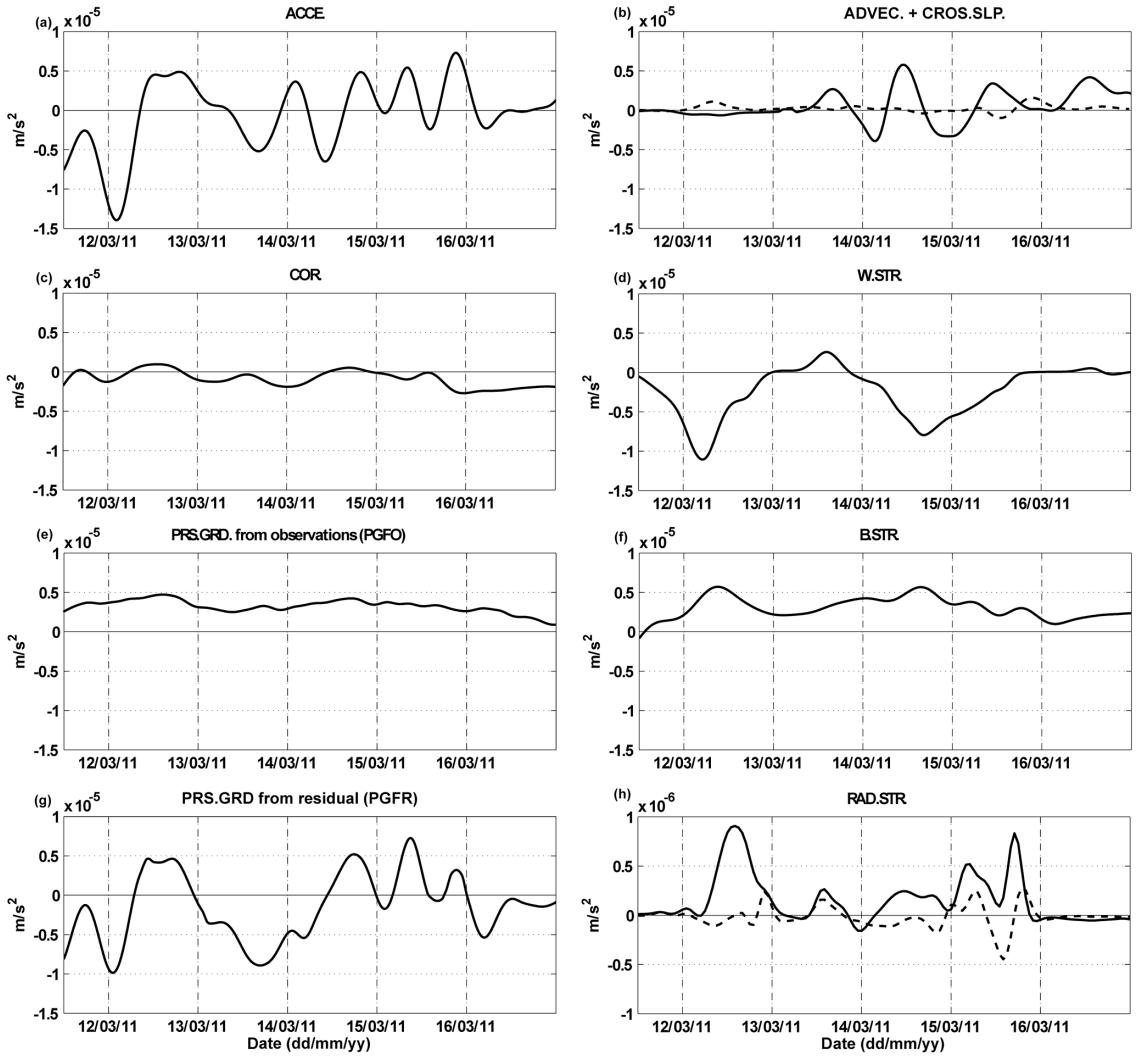

Figure 4. Estimates for the along-shelf momentum terms at 25 m. Left-hand-side terms of Eq. (1): **(a)** acceleration terms (ACCE. $\delta v/\delta t$), **(b)** advective (solid line, ADVEC., $\delta v^2/\delta y + \delta(vu)/\delta x$) and cross-slope (dashed line, CROS.SLP., $(uv/H)\ \delta H/\delta x$) terms estimated from the currents at the neighboring ADCP locations and **(c)** Coriolis term (COR., fu). Right-hand-side terms of Eq. (1): **(d)** wind stress term (W.STR., $\tau_{ys}/\rho H$), **(e)** pressure-gradient force from observations (PGFO term, $g\delta\eta/\delta y$), **(f)** bottom stress term (B.STR., $\tau_{yb}/\rho H$), **(g)** pressure-gradient force from residual (PGFR) and **(h)** radiation stress term (RAD.ST., $(1/\rho H)\delta S_{xy}/\delta x$ solid line, and $(1/\rho H)\ \delta S_{yy}/\delta y$ dashed line). Notice the change in the vertical scale in panel **(h)**. The data used for estimating the momentum terms have been low-pass filtered, with a cutoff period of 12 h. The date indicates 00:00 UTC.

few hours before the maximum winds (12 March 05:00 and 12 March 7:00 UTC). After the first wind peak, the acceleration decreased rapidly and changed sign, becoming small but positive during the remaining of the wind pulse. Something similar happened during the second wind peak, but this time characterized by several fluctuations, with acceleration peaks occurring about every 24 h or less (Fig. 4a).

The bottom stress (B.STR. in Eq. 1) is estimated using a linear drag law (Lentz and Winant, 1986):

$$\tau_{ys} = \rho\, r\, v_{\mathrm{b}}, \tag{2}$$

where r is the linear drag coefficient, ρ is density and v_{b} is the near-bottom velocity (measured at about 1 m from the sea bottom). The estimation of the drag coefficient depends on the water depth and the along-shelf velocity; large fluctuations in the value of r have been found to occur as the prevalent momentum terms change (Lentz et al., 1999). Typical values for water depths of a few tens of meters are between 10^{-3} and $10^{-4}\,\mathrm{m\,s^{-1}}$ (e.g., Winant and Beardsley, 1979). In our analysis, the drag coefficient was close to $10^{-3}\,\mathrm{m\,s^{-1}}$, estimated from the momentum balance evolution as explained below. Linear drag formulations are well established for steady-state conditions but might cause misrepresentations during transient conditions (such as during the passage of a storm). We not only use the linear formula-

tion as a first estimate of the size of the frictional terms but also consider the potential effect of non-linear friction (Appendix A). The time series for the bottom stress term had peak values at times of maximum along-shelf flow, almost immediately after the peak wind stress (Fig. 4e).

The wave-induced mass fluxes (RAD.STR. in Eq. 1) are estimated as follows:

$$S_{xy} = E\frac{c_g}{c}\sin\phi\cos\phi, \tag{3}$$

$$S_{yy} = E\left[\frac{c_g}{c}\left(1+\sin^2\phi\right)-\frac{1}{2}\right], \tag{4}$$

where the wave energy is computed as $E = \rho_0 g H_{sig}^2/16$, with H_{sig} as the significant wave height, ϕ the wave direction of propagation, and c_g and c, respectively the (linear theory) group and phase velocity at the peak wave frequency. Model radiation stress gradients are then estimated from two adjacent numerical cells in the proximity of A2 that considered the propagation of wave conditions measured at A3. The peak values in significant wave height (about 2.5 m), and hence in the radiation stresses, occurred slightly after the maximum winds because of swell effects (Fig. 4h). The radiation stress terms were 1 order of magnitude smaller than the dominant frictional and acceleration terms.

No direct estimate of the along-shelf pressure-gradient force (PRS.GRD. in Eq. 1) can be obtained from the data. The ADCP recorded the pressure in the water column but the distances between ADCPs are not appropriate to capture the along-shelf sea-level variability, as the signal-to-noise ratio is not adequate. Hickey (1984) pointed out that, for spatial scales of the same order of magnitude as the external Rossby radius (about 100 km in the Catalan Sea), the expected sea-level gradient would be only a few centimeters. In our case, the sea-level variations recorded by the pair of pressure sensors in A1 and A2 (separated by only a few kilometers) were of the same order as the accuracy of the devices (order millimeters). As an alternative approximation, an observed pressure-gradient force (PGFO) may be computed using data from a sea-level gauge located in the harbor of Blanes (approximately 64 km to the north; Fig. 1) and the ADCP pressure sensor at A2. This along-shelf pressure gradient remained positive during the entire storm, meaning a downwind accumulation of water, and was reinforced during the two wind peaks (Fig. 4e).

Additionally, we may calculate this along-shelf pressure-gradient force as the residual from the momentum balance equation (PGFR) as follows:

$$\mathrm{PGFR} = \frac{\partial\bar{v}}{\partial t} + \frac{\partial\bar{v}\bar{v}}{\partial y} + \frac{\partial\bar{u}\bar{v}}{\partial x} + \frac{\bar{u}\bar{v}}{H}\frac{\partial H}{\partial x} + f\bar{u} - \frac{\tau_{ys}}{\rho H} + \frac{\tau_{yb}}{\rho H} + \frac{1}{\rho H}\left(\frac{\partial S_{yy}}{\partial y} + \frac{\partial S_{xy}}{\partial x}\right). \tag{5}$$

Maza et al. (2006) used a similar approach to compute the pressure-gradient force when the sea-level gradient was not available from observations. In our case, the value of r is estimated iteratively until the maximum PGFR matched the maximum PGFO during the first peak of the storm (Fig. 4g). This strategy resulted in an observationally based r value that is consistent with the evolution of the momentum balance. The resulting coefficient is $8.5 \times 10^{-4}\,\mathrm{m\,s^{-1}}$, comparable to values computed from observations at similar depths (Winant and Beardsley, 1979).

Both the observed and residual pressure-gradient time series (PGFO and PGFR) reproduce the force direction of the sea-level slope during the wind stress peaks (Fig. 4d). The PGFR includes a contribution by a direct response to the local wind forcing (for instance during 13 March), which is not immediately obvious in PGFO. During the wind peaks, the positive pressure-gradient force partially counterbalanced the wind stress in a manner consistent with other observational studies (Lee et al., 1984; Lentz, 1994; Fewings and Lentz, 2010). Despite its potentially large uncertainty, we use PGFR in the analysis of the momentum balance evolution because it is consistent with the estimates for the other momentum terms.

3.3 Momentum balance near the mid-shelf

The cross-shelf variability of the along-shelf momentum is estimated by comparing the inner-shelf results with the momentum terms at 50 m water depth. The acceleration and bottom stress follow a pattern similar to the one observed at 24 m (Fig. 5). During the first wind peak, the acceleration responded to the wind stress, with its maximum occurring before the maximum winds. The maximum bottom stress, as at 24 m, occurred a few hours after the maximum winds. During the second peak, the situation was less clear than at 24 m, with substantial oscillations in the acceleration and bottom stress. The bottom stress reached a minimum toward the end of the negative wind stress pulse.

From the velocities observed at A3, we estimate the surface and bottom frictional forces, the acceleration and the Coriolis force (Fig. 5). The surface stress term is estimated with the local wind measured at the CSO, scaled with the corresponding water depth. The non-linear terms cannot be estimated due to the lack of additional measurements at 50 m, necessary to assess the along-shelf gradient. Thus, as the advective and wave-radiation terms are not available, we estimate the pressure gradient as a residual that results from combining acceleration, Coriolis and wind and bottom friction ($\mathrm{PGFR_{ACCE+COR+FRIC}}$):

$$\mathrm{PGFR_{ACCE+COR+FRIC}} = \frac{\partial\bar{v}}{\partial t} + f\bar{u} - \frac{\tau_{ys}}{\rho H} + \frac{\tau_{yb}}{\rho H}. \tag{6}$$

In next section, we examine the relation of this residual with the other terms at 50 m depth, to explore the changing role of the Coriolis force with water depth.

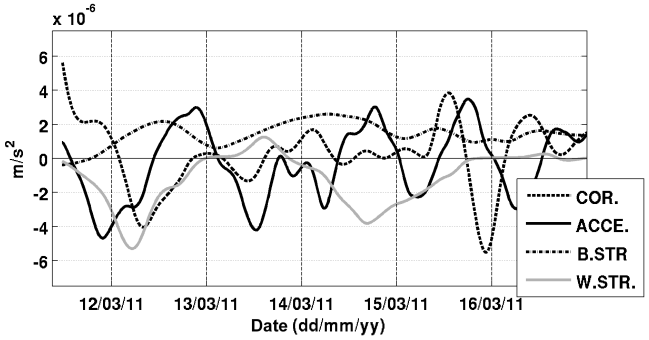

Figure 5. Estimates for the along-shelf momentum terms at 50 m. Left-hand-side terms of Equation 1: acceleration terms (ACCE. $\delta v/\delta t$) and Coriolis (COR. fu). Right-hand-side terms of Equation 1: wind stress term (W.STR. $\tau_{ys}/\rho H$) and bottom stress term (B.STR. $-\tau_{yb}/\rho H$). The data used for estimating the momentum terms have been low-pass filtered with a cutoff period of 12 h. The date indicates 00:00 UTC.

4 Discussion

4.1 Momentum evolution in the inner shelf

From the estimated along-shelf momentum terms, we conclude that the primary balance at 24 m (Fig. 4) took place between acceleration, wind stress, bottom friction, momentum advection and pressure force gradient. The Coriolis force and the radiation stress played secondary roles in the momentum balance. In particular, the radiation stresses were 1 order of magnitude smaller than the dominant acceleration, pressure gradient and frictional terms, consistent with other studies that ignored wave forcing outside the surf zone (Lentz et al., 1999; Fewings and Lentz, 2010). In a region 150 km north of our study area, in water depths of 28 m off the Tet River, Michaud et al. (2012) confirmed numerically that the wave effects on the inner-shelf circulation are relatively small even during a storm event.

While our estimates present some uncertainty as a result of instrumental inaccuracies and the intrinsic assumptions in the estimation of the terms, we expect them to be reasonable approximations to the relative size of the dominant terms in the time-varying along-shelf momentum balance. In this section, we combine the wind and velocity observations with the along-shelf momentum estimates to further analyze the inner-shelf response to the changing winds.

During the first peak (12 March), as the wind stress increased, the acceleration term initially became more negative and the bottom stress more positive, as expected from the direction of the flow (Fig. 4a). The peak in the acceleration term occurred 4 h before the wind maximum, as a result of the enhanced frictional dissipation and a rapid change in the residual pressure-gradient force (PGFR), from negative to positive values (Fig. 4a, f and g). The change in the sign of PGFR, indicative of downwind water accumulation, was abrupt, being responsible for switching the acceleration from negative to positive at about 10:00 UTC, hence setting the size and timing of the maximum along-shelf current (Fig. 3d).

During the calm period (13 March), the PGFR once again reversed, likely caused by a relaxation after the first wind peak. The acceleration remained close to zero until 13 March 10:00 UTC and then turned negative, despite the appearance of weak northeast winds. The negative acceleration started at the time when onshore winds were observed (Fig. 3a). The intensification of the southwestward PGFR was locally reflected by a leveling of the sea surface throughout 13 March (Fig. 3e). The sequence of events is consistent with the intensification of a southwestward flow probably in cross-shelf geostrophic balance. During 14 March, when both along- and cross-shelf winds were weak, some nearshore water was progressively released, first through a two-layer baroclinic cross-shelf flow and then by offshore flow in the entire water column (Fig. 3c).

The along-shelf momentum balance during the second wind peak shared some characteristics with the balance during the first wind peak but also displayed important differences. The acceleration term and the PGFR were enhanced following the increase in wind stress, with the along-shelf velocity reaching a maximum at the time of the second wind peak. However, the second wind event also had substantial fluctuations in the acceleration, advective, bottom friction, Coriolis and PGFR terms (Fig. 4). The fluctuations appear as a moderate increase in energy at the 12–16 h band in the wavelet analysis for the depth-averaged currents at station A2 (Fig. 6). These oscillations are consistent with fluctuations in the lowest part of the water column in the cross-shelf velocities (Fig. 3c), and could be explained as a transient coastal current response to the sudden enhanced wind stress in the form of inertio-gravity waves (Kundu et al., 1983; Tintoré et al., 1995). These waves are associated with near-inertial motions resulting from the flow adjustment at the coast. Another plausible explanation of these oscillations is the generation of internal waves dispersed from the surface (wind-mixed layer) to larger depths in the lee of the storm (Gill, 1982; Kundu and Thompson, 1985) or fast coastal Kelvin waves (Csanady, 1982; Gill, 1982). Their proper characterization would require additional observations in the cross- and along-shelf directions jointly with more detailed information of the stratification in the water column before and after the storm.

The along-shelf velocity spectral and wavelet analyses also show the existence of fluctuations with a dominant periodicity of about 2 days, although only significant for 14 and 15 March (Fig. 6). Sub-inertial fluctuations in that band of the spectrum may reflect the propagation into the study area of free coastal waves generated elsewhere during the first part of the storm. The propagation of topographic waves is briefly considered in Appendix B, using the Csanady (1982) coastal-strip model to assess the magnitude of the oscillations for a

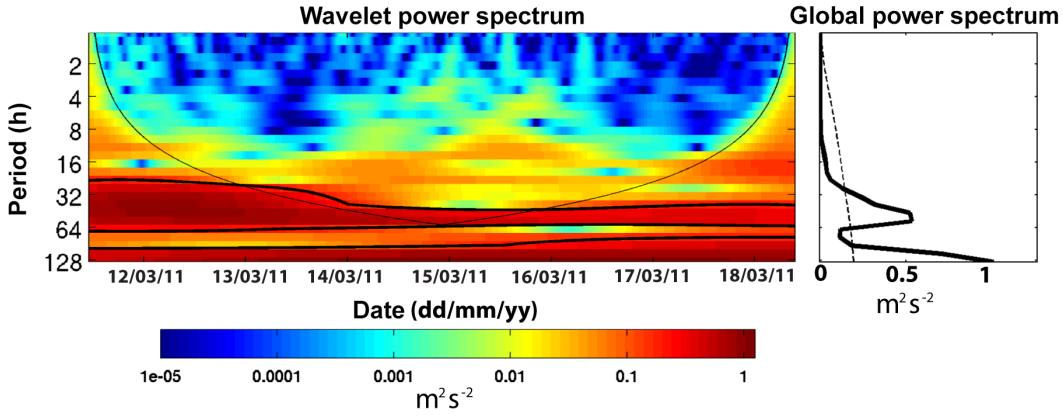

Figure 6. (Left) wavelet analysis and (right) spectral analysis for the depth-averaged currents at station A2. The solid thin line in the wavelet power spectrum shows the energy values that exceed the significance level; similarly, the dashed line in the global power spectrum shows the significance level. The date indicates 00:00 UTC.

linear and frictionless coastal band. The theoretical lowest-mode topographic waves have a period of about 32 h, which is similar to the dominant period as deduced from the spectral and wavelet analyses (Fig. 6). Observed sea-level oscillations (Fig. 3e), as large as 0.05 m on timescales of about 1–2 days, gave rise to velocities of about 0.3 m s^{-1} (Fig. 3c). Jordi et al. (2005) described the existence of topographic waves in the NW Mediterranean Sea, which propagated southwest. Due to our limited observations, additional measurements and numerical modeling efforts (e.g., Brink and Chapman, 1985) are necessary to properly characterize the relevance of topographic waves during storms.

The differences between the observed and residual pressure-gradient forces, PGFO and PGFR, are striking (Fig. 3). The PGFR is necessary to balance the flow yet it differs substantially from the pressure gradient as calculated from the A2 and Blanes sea-level gauges (64 km apart). Hence, we may interpret the PGFR as composed of two contributions: (1) a rapid coastal response to the along- and cross-shelf wind forcing, and (2) a relatively slow sea-level adjustment to the propagating storm. Our interpretation is that the PGFO corresponds to the second, relatively smooth, contribution, which would drive the flow in the absence of waves (as it occurs during the first wind event).

Our analysis highlights the importance of the initial conditions (whether the system starts from rest or not) and the complexity of the momentum fluctuations during the development of the storm. A comparison of the temporal evolution of the momentum terms during both wind peaks shows that the role of the acceleration and advective terms is quite different. During the first peak, the advective terms are relatively small as a result of the linear response of the pressure gradient and bottom stress to the wind forcing. After the first peak, however, the acceleration and advective terms display fluctuations that may reflect transient waves. Hence, the along-shelf velocity during the second peak is the cumulative effect of a local response to wind stress combined with the arrival of waves that barely feel the effect of bottom friction.

4.2 Frictional adjustment and Ekman depth in the inner shelf

During the first wind peak, the increase in along-shelf velocity enhanced the bottom stress, which eventually balanced the joint effect of wind stress and along-shelf pressure gradient, therefore achieving a complete frictional adjustment. A measure of the frictional adjustment time can be extracted from the observations, considering the cross-zero momentum and inflexion points in the time series. During the first peak (12 March), the flow started from near rest and the non-linearities were small. After the first peak, the momentum balance was affected by fluctuations in the acceleration and advection terms responding to the cross-shelf slope momentum term. Hence, a maximum value for the frictional adjustment time is estimated as the time between zero and maximum bottom stress during the first wind pulse, or about 14 h (from 11 March 20:00 UTC to 12 March 10:00 UTC). This frictional adjustment time doubles the frictional time as computed from the linear drag law of the bottom stress term ($t = H/r = 7.8$ h) and is consistent with typical values from similar depths. For instance, Winant and Beardsley (1979) provided estimates ranging between 7 and 26 h at depths between 28 and 31 m.

To provide a framework for the frictional time, we consider the linearized analytical model from Csanady (1982), applied to the first wind peak period. The along-shelf velocity response to a steady wind stress, considering only bottom friction, is controlled by the following expression:

$$\frac{\partial \bar{v}}{\partial t} = \frac{\tau_{ys}}{\rho H} - \frac{\tau_{yb}}{\rho H}. \quad (7)$$

Solving this equation for a quadratic drag law (Appendix A), we obtain an exponential relation with a characteristic fric-

tional adjustment timescale (t_f).

$$t_f = \frac{H}{2\sqrt{\frac{\tau_{ys}}{\rho} C_{\mathrm{da}}}}, \tag{8}$$

where C_{da} is a bottom drag coefficient associated with the depth-averaged velocity. For a value of wind stress of 0.12 Pa (averaged value during the first peak), t_f is 13 h. This magnitude agrees well with the frictional adjustment time estimated from observations (about 14 h) and confirms the short response time of locally generated along-shelf currents. Therefore, the frictional timescale is shorter than the adjustment timescale for geostrophic balance to take place, of the order of an inertial oscillation period, $f^{-1} = 18.15$ h. This result supports the view that, during the passage of the storm, the locally generated flow at 24 m is regulated by bottom dissipation; a result that is consistent with the reduced contribution of the Coriolis term to the local along-shelf momentum balance.

It is important to point out that the sea surface adjustment time is similar to the time period between the two wind peaks. The along-shelf momentum generated by the first wind pulse did not have sufficient time to dissipate before the second wind peak arrived. In our case, this is further complicated by the potential arrival of upstream waves. This progressive adjustment may be appreciated in the time evolution of the sea surface, where the sea level approached some near-equilibrium value towards the end of each wind pulse (Fig. 3e). The sea-level time series also illustrates that the adjustment is characterized by at least two separate components: one responding to local wind forcing and the local response to remotely generated waves and another, much slower, associated with the sea-level adjustment at scales of the order of the external Rossby radius (Hickey, 1984), about 100 km in the Catalan shelf.

The short frictional adjustment time is consistent with the study site being part of the inner shelf during the storm. The inner shelf is defined as the region where the combined surface and bottom boundary layers occupy the entire water column (Lentz, 1994). Obviously, the boundaries of the inner-shelf region vary in time depending on the intensity of the forcing mechanism. The bottom and surface Ekman depth can be obtained from empirical formulations such as (Weatherly and Martin, 1978)

$$\delta = \frac{1.3\, u^*}{\sqrt{N f}}, \tag{9}$$

where $u^* = (\tau_s/\rho)^{1/2}$ is the friction velocity, τ_s is the surface/bottom stress magnitude and $N^2 = g\,\mathrm{d}\rho/\mathrm{d}z$ is the squared buoyancy frequency. The time evolution of the surface and bottom Ekman layers (Fig. 7) is computed iteratively (as N depends on the vertical position within the water column). The buoyancy frequency for Eq. (9) is estimated using the CTD measurements during 17 March (2 days after the storm; Grifoll et al., 2012). The N values are estimated to be $0.03\,\mathrm{s}^{-1}$ for the surface layer and $0.005\,\mathrm{s}^{-1}$ for the bottom layer. The transient nature of the storm will cause some differences in the level of stratification, especially in the surface layer, but the relative size of the terms will remain mostly unchanged. Periods with less energetic wind conditions exhibit smaller wind stress; therefore, the relative importance of the Coriolis term increases at 24 m (Grifoll et al., 2012). Our results show that the boundary layers overlapped most of the time during the storm event (Fig. 7). Even though the applicability of Eq. (9) has been questioned for areas influenced by freshwater discharge (Garvine, 2004; Dzwonkowski et al., 2014), the calculated Ekman layer depths are consistent with the importance of the frictional terms in the along-shelf dynamics.

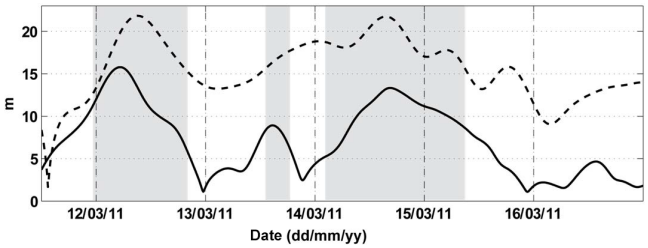

Figure 7. Estimates of the surface (continuous line) and bottom (dashed line) Ekman depths (m). The gray patches show the periods where the sum of the surface and bottom Ekman depths exceeded 24 m (the water depth at station A2). The date indicates 00:00 UTC.

4.3 Cross-shelf variability of the along-shelf momentum terms

The cross-shelf variability of the along-shelf momentum is investigated with the help of the momentum terms calculated at 50 m water depth. The frictional adjustment time, as observed through the evolution of the momentum terms at 50 m, exhibited a 4 h lag when compared with the frictional adjustment time at 24 m (Sect. 4.1), likely caused by the time delay in the vertical transfer of momentum. The linear drag coefficient is calculated following the same approach as for the analysis at 24 m, now adjusting the $\mathrm{PGFR}_{\mathrm{ACCE+COR+FRIC}}$ term (without advection terms) to the observed value (PGFO) for the first peak of the storm. The resulting value, $r = 7.3 \times 10^{-4}\,\mathrm{m\,s}^{-1}$, is close to the value of r for the inner shelf ($8.5 \times 10^{-4}\,\mathrm{m\,s}^{-1}$). This supports our conclusion that, during the first storm peak, the along-shelf momentum balance was controlled by the combination of local acceleration, Coriolis and friction, while the advective, Coriolis and radiation stress terms played a secondary role.

The relative ratio of the fluctuations (standard deviations) in the acceleration and wind stress terms, $\left(\frac{\rho_0 H\, \partial \bar{v}/\partial t}{\tau_{ys}}\right)$, increases offshore (from 1.10 at 24 m to 1.36 at 50 m). These values are larger than estimates from other shelves (Lentz

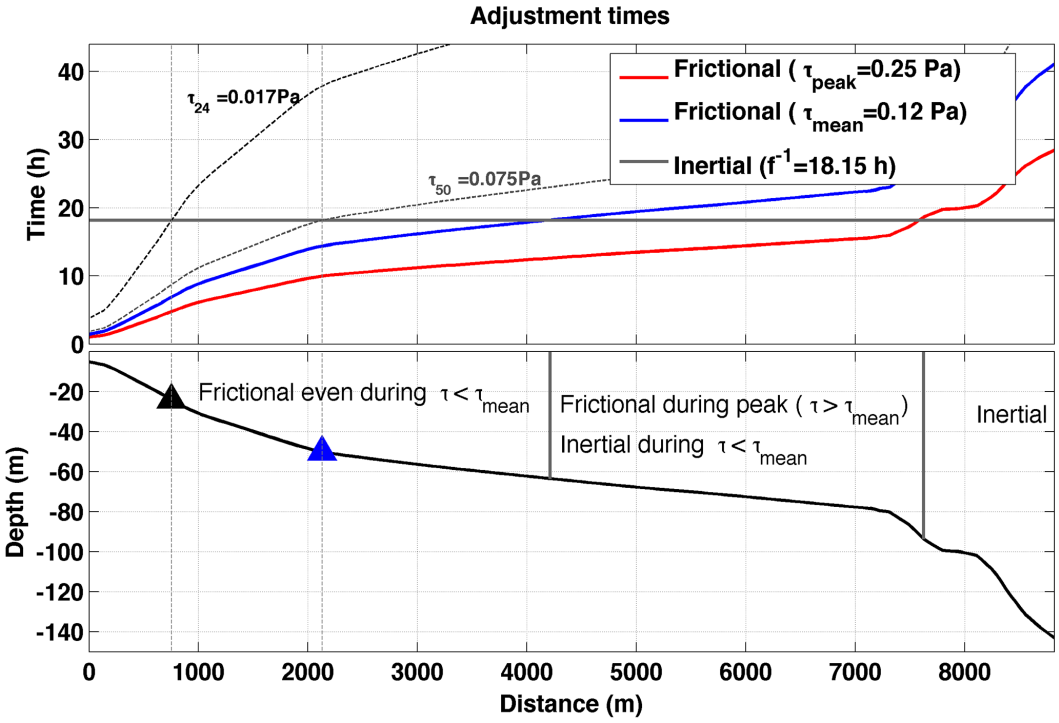

Figure 8. (Top panel) cross-shelf transect of the frictional adjustment times for several along-shelf wind stresses (τ) together with the inertial time off the city of Barcelona (18.15 h, grey solid line). The cross-shelf variation of the frictional adjustment time (computed following Eq. 8) is shown for storm peak conditions (red line) and averaged storm conditions (blue line). The two dotted lines correspond to wind stresses such that the frictional and inertial times become equal at 24 m (t_{24}) and 50 m (t_{50}) water depth. (Bottom panel) the location of the inertial, frictional and transition zones for the peak and mean storm conditions. The ADCP locations at 24 m and 50 m are indicated with black and blue triangles, respectively.

and Fewings, 2012): in the Middle Atlantic Bight, around 0.3 and 0.5 at 25 and 50 m, respectively; and in the West Florida Shelf, 0.5 and 1 for 25 and 50 m, respectively. The larger values found in the Catalan shelf are ascribed to the enhanced acceleration during the storm.

The size of the Coriolis term at 50 m increases in comparison to the size of this term estimated at 24 m water depth. The standard deviation of the Coriolis term also increases offshore, from 9.6×10^{-7} m s^{-2} at 24 m to 1.5×10^{-6} m s^{-2} at 50 m. The ratio of the fluctuations between the Coriolis and wind stress terms, $\left(\frac{\rho_0 H f \tilde{u}}{\tau_{ys}}\right)$, increased from 0.3 at 24 m to 1.3 at 50 m water depth. Lentz and Fewings (2012) presented ratios around 0.4 for the Middle Atlantic Bight and West Florida Shelf at 25 m, and between 2 and 3 at 50 m depth.

The increasing/decreasing importance of the Coriolis/bottom-frictional terms responds to a switch towards the geostrophic balance, typical in the transition from the inner to the mid-shelf. With increasing depth, the frictional effects decrease in the along-shelf momentum balance. Lee et al. (1984) observed that the Coriolis term doubled from 28 to 75 m water depth in the South Atlantic Bight (USA), with progressively smaller frictional terms. At the start of our study period (11 March 2011, Fig. 5), the 50 m water depth Coriolis term was larger than the other terms, suggesting a geostrophic balance during the calm period.

During the storm period, the $\mathrm{PGFR_{ACCE+COR+FRIC}}$ term at 50 m is moderately correlated with the Coriolis term ($R = 0.55$ with 95 % confidence level). This correlation suggests that the dynamic response at 50 m includes a large geostrophic component, of greater relevance than at 24 m, where the PGFR is less correlated with Coriolis ($R = 0.33$ with 95 % confidence level). However, the acceleration and frictional terms, and likely the non-linear terms, also play an important role at 50 m water depth during the storm; for example, the acceleration terms at 24 and 50 m are also moderately correlated ($R = 0.64$ with 95 % confidence level). Michaud et al. (2013), from observations in the Gulf of Lion (275 km north of our study area, Fig. 1) at 65 m depth, also emphasized the importance of the wind-induced geostrophic currents during a storm.

We may finally compare the cross-shelf changes of the frictional and geostrophic terms in the along-shelf momentum balance (Fig. 8). Their relative importance can be explored by comparing the bottom frictional time (Eq. 8) with the inertial time ($f^{-1} = 18.15$ h). During the peak of the

storm (surface stress $\tau = 0.25$ Pa), the frictional and inertial times are equal for water depths of 94 m; for the average stress of the storm (surface stress $\tau = 0.12$ Pa) this happens for water depths of 64 m. Thus, the frictional effects dominated for depths up to around 60 m, causing our current meters to be located in regions controlled by inner-shelf dynamics during the entire storm. For the frictional and inertial times to be the same, the wind stress would have to be 0.075 Pa at 50 m and 0.02 Pa at 24 m. Therefore, the Coriolis term is relatively not important at 24 m except for very low surface stresses, such as during the calm period between the two storm pulses (0.02 Pa); during those times other terms, like the pressure-gradient force, will dominate the along-shelf momentum balance (Grifoll et al., 2013).

5 Conclusions and final remarks

We have assessed the effects of the passage of a storm over the inner Catalan shelf (NW Mediterranean Sea) on the along-shelf momentum balance. At 24 m water depth, a primary momentum balance between acceleration, pressure-gradient and frictional forces (surface and bottom) is established. The Coriolis and the wave-induced momentum terms play a second-order role in the momentum balance. Our estimates for the frictional adjustment time and Ekman depth confirm the prevalence of the frictional response of the flow at 24 m. The increasing importance of Coriolis at 50 m corresponds to a shift towards the geostrophic behavior, characterizing the transition from the inner to the mid-shelf.

The storm (12–15 March 2011) had two separate wind peaks that caused currents with some similarities but also important differences. The main similarity was the local response to wind forcing, with the along-shelf flow (towards the southwest) accelerating to a maximum shortly after the wind peak, at a time when the joint effect of bottom stress and a northeastward pressure-gradient force (arising from downwind water set up) compensated for the decreasing wind stress. Such a response was more obvious during the first peak (13 March), as the system started from a condition of weak along-shelf flow. During the relatively calm period between both wind peaks (14 March), the pressure-gradient force turned toward the southwest and the flow remained in that direction. During this period, the winds were weakly onshore, likely setting a cross-shelf geostrophic balance. By the end of the calm period, and lasting through the second wind peak (15 March), the momentum balance was characterized by the appearance of fluctuations with both super-inertial (12–16 h) and sub-inertial (1–2 days) periods. During the second wind peak, the temporal sequence of increased acceleration followed by opposing bottom stress and pressure gradient reoccurred, but with the along-shelf flow largely influenced by the sub-inertial (likely topographic) waves, with velocity amplitudes as large as $0.3\,\mathrm{m\,s^{-1}}$. These waves remained active even when the second wind peak had ended.

In our analysis, we have focused on the shelf response to a single twin storm, where extensive observational data were available. However, northeasterly energetic wind events are common during spring and fall in the Catalan shelf; therefore, similar events are expected on a yearly basis. The extrapolation of our results to other shelves depends on physical variables such as stratification, river discharge and remote sea-level forcing. In relatively low-energy shelves, such as the Catalan shelf, it is plausible that two-peak storms be commonly characterized by a sequence of a linear response followed by a subsequent non-linear behavior.

Early investigations (e.g., Scott and Csanady, 1976) pointed out that tidally driven fluctuations hinder the analysis of the wind-induced fluctuations over relatively shallow depths, where the frictional adjustment time may be similar or shorter than the tidal period. In these environments, for typical wind events, the wind-forcing, tidal and frictional periods are all comparable; in particular, the semidiurnal and frictional times become similar at depths of about 60 m (Csanady, 1982). In contrast, the micro-tidal nature of Catalan shelf has allowed us to investigate in detail the shelf response at temporal scales shorter than previously investigated for the inner shelf.

Appendix A: Frictional adjustment time for linear and quadratic formulations

A simple model to determine the frictional time adjustment was presented by Csanady (1981), based on the transport momentum equation in the along-shelf direction:

$$\frac{\partial V}{\partial t} + fU = -gH\frac{\partial \eta}{\partial y} + u^{*2} - \frac{\tau_{yb}}{\rho}, \tag{A1}$$

where the transport is

$$U = \int_{-H}^{0} u\,\mathrm{d}z, \tag{A2a}$$

$$V = \int_{-H}^{0} v\,\mathrm{d}z, \tag{A2b}$$

and the frictional velocity is given by

$$u^* = \sqrt{\frac{\tau_{ys}}{\rho}}. \tag{A3}$$

Under the assumption that the depth distribution is only a function of the cross-shelf coordinate, we neglect the along-shelf pressure gradients. Also, the coastal constraint near the coast implies $U = 0$. These conditions lead a frictional balance between the acceleration and the wind and bottom stresses:

$$\frac{\partial V}{\partial t} = u^{*2} - \frac{\tau_{yb}}{\rho}. \tag{A4}$$

The bottom stress was parameterized by Csanady (1981) using a quadratic drag law equation as a function of the depth-averaged current (V/H):

$$\frac{\tau_{yb}}{\rho} = C_{\mathrm{da}}\left(\frac{V}{H}\right)^2. \tag{A5}$$

Integrating, the solution for the along-shelf transport follows an exponential equation

$$V = \frac{u^* H}{\sqrt{C_{\mathrm{da}}}}\left(\frac{1-\exp\left(-2u^* t\sqrt{C_{\mathrm{da}}}/H\right)}{1+\exp\left(-2u^* t\sqrt{C_{\mathrm{da}}}/H\right)}\right), \tag{A6}$$

with an e-folding timescale of

$$t_f = \frac{H}{2\sqrt{\frac{\tau_{ys}\,C_{\mathrm{da}}}{\rho}}}. \tag{A7}$$

Alternatively, we may consider the bottom frictional term to depend linearly on the depth-averaged current:

$$\frac{\tau_{yb}}{\rho} = r\left(\frac{V}{H}\right). \tag{A8}$$

In this case, the solution follows again an exponential solution:

$$V = \frac{u^{*2} H}{r}\left(1-\exp\left(-\frac{r}{H}t\right)\right), \tag{A9}$$

where the e-folding timescale is H/r, as expected according to the lineal parameterization of the bottom stress in Eq. (2). Linear and quadratic derived frictional time expressions have the same physical meaning, with e-folding times proportional to the water depth and inversely proportional to bottom stress parameter (r or C_{da}). For the linear and quadratic formulations, at long times the depth-averaged velocities tend asymptotically to $\frac{u^*}{\sqrt{C_{\mathrm{da}}}}$ and $\frac{u^{*2}}{r}$, respectively, which are the velocities required for bottom stress to balance the wind stress.

Appendix B: Topographic waves over the continental shelf

Here, we follow Csanady (1982, Sect. 4.5) to estimate the size of the coastal propagating anomalies. We look at the non-forced propagation of a sea surface perturbation, with elevation η, generated at some earlier time in some upstream location along the coast. We keep the same coordinate convention as in the main text, with (x, y), respectively directed cross shelf and along shelf (positive offshore and to the northeast). Following Grifoll et al. (2013), we let the dominant terms in the cross-shelf direction to be in geostrophic balance. Hence, the linearized depth-averaged momentum- and mass-conservation equations for non-stratified and frictionless conditions are (dropping overbars):

$$-fv = -g\frac{\partial \eta}{\partial x}, \tag{B1}$$

$$\frac{\partial (vH)}{\partial t} + fuH = -gH\frac{\partial \eta}{\partial y}, \tag{B2}$$

$$\frac{\partial (uH)}{\partial x} + \frac{\partial (vH)}{\partial y} = -\frac{\partial \eta}{\partial t}. \tag{B3}$$

Let us idealize our coastal ocean as having the water depth independent of the along-shelf distance, $H = H(x)$. Taking the curl of the momentum equations and using the mass-conservation equation leads to the following vorticity equation (constant f condition)

$$\frac{\partial^2 (vH)}{\partial t\,\partial x} - f\frac{\partial \eta}{\partial t} = -g\frac{\mathrm{d}H}{\mathrm{d}x}\frac{\partial \eta}{\partial y}. \tag{B4}$$

In the cross-shelf direction the change in water depth is much greater than the change in surface elevation (the equivalent of assuming the rigid lid approximation for the mass-conservation equation), i.e., $\frac{\partial (vH)}{\partial x} \gg \partial \eta/\partial t$. Hence, we may safely neglect the second term in the left-hand side of Eq. (B4) so that, using Eq. (B1), we get

$$\frac{\partial^2}{\partial t\,\partial x}\left(H\frac{\partial \eta}{\partial x}\right) + f\frac{\mathrm{d}H}{\mathrm{d}x}\frac{\partial \eta}{\partial y} = 0. \tag{B5}$$

We need two boundary conditions to solve this equation. The first one comes from the condition of no-normal flow at the coast; from Eq. (B2), and with the help of Eq. (B1), we obtain

$$\frac{\partial^2 \eta}{\partial t \partial x} + f \frac{\partial \eta}{\partial y} = 0, \qquad \text{at } x = 0. \tag{B6}$$

The second condition may be simply specified from the requirement of a finite-size perturbation; from Eq. (B1) this is equivalent to setting that far enough from the coast the elevation of the perturbation tends to zero:

$$\frac{\partial \eta}{\partial x} = 0 \qquad \text{at } x = L_x. \tag{B7}$$

Here, we choose L_x to be the width of the continental shelf (i.e., the offshore extent of the perturbation is limited by the width of the coastal band). For our study, we take this to be the characteristic width of the continental shelf north of Barcelona, or about 40 km.

The solution of Eq. (B5) subject to the boundary conditions (B6) and (B7) is obtained through separation of variables, $\eta(x, y, t) = \phi(y, t)\,\chi(x)$. The equation for $\phi(y, t)$ becomes

$$\frac{\partial \phi}{\partial t} - c_i \frac{\partial \phi}{\partial y} = 0, \tag{B8}$$

where c_i is the separating constant. The general solution corresponds to a wave propagating in the negative y direction (in our case, towards the southwest), $\phi(y + c_i t)$, showing that c_i corresponds to the phase speed of the traveling perturbation.

Following Csanady (1982), let the water depth be a linear function of the cross-shelf distance, $H(x) = x H_0 / L_x \equiv sx$, where s is the slope. The equation for $\chi(x)$ becomes

$$\xi \frac{\mathrm{d}^2 \chi}{\mathrm{d}\xi^2} + \frac{\mathrm{d}\chi}{\mathrm{d}\xi} + \chi = 0, \tag{B9}$$

where $\xi \equiv fx/c_i$. The boundary condition at the coast becomes $\left(\frac{c_i}{f}\right)\frac{\mathrm{d}\chi}{\mathrm{d}x} + \chi = 0$, and the condition at $x = L_x$ turns into $\frac{\mathrm{d}\chi}{\mathrm{d}x} = 0$. Equation (B9) together with these boundary conditions is an eigenvalue problem, with different solutions for a discrete number of positive c_i values. The solution that satisfies the boundary condition at the coast is $\chi = A J_0\left(2\xi^{1/2}\right)$, where J_0 is a Bessel function of order 0, and A is a constant. The boundary condition at $x = L_x$ sets the possible c_i values, those that satisfy $J_1\left[2(fl/c_i)^{1/2}\right] = 0$, where J_1 is a Bessel function of order 1. The faster wave corresponds to $c_1 = fL_x/3.67$, having the simplest structure: maximum velocity at the coast that decreases to zero at L_x.

From Eq. (B1), the along-shelf velocity is $v = -(gA\phi)/(c_i f x)^{1/2} J_1\left(2\sqrt{\frac{fx}{c_i}}\right)$. The maximum velocity takes place at the coast, given by $v = -\frac{(gA\phi)}{c_1} = -(3.67 gA\phi)/(fL_x)$, its magnitude depending on the elevation $A\phi$ at the coast. In Fig. 3e, we see changes in elevation as large as 0.05 m taking place on timescales of 1–1.5 days, which would represent velocities of about $0.3\,\mathrm{m\,s^{-1}}$, which is in fair agreement with the observed oscillations (Fig. 3b).

The periodicity of these perturbations depends on the size of the region where they are generated, which sets the along-shelf wavenumber $k = 2\pi/L_y$. The shortest period corresponds to the fastest propagating perturbations, which are also the ones that result in the largest along-shelf velocities; it turns out to be $T \equiv \frac{2\pi}{\omega} \equiv \frac{2\pi}{(c_1 k)} = \frac{3.67 L_y}{fL_x}$. If we choose L_y to be 120 km, or about the size of the domain with maximum gradients in sea-level pressure (and hence maximum winds) (Fig. 2), we get $L_y/L_x \cong 3$ and the period is about 32 h. This number is to be taken only as a very rough estimate but yet it suggests that some of the energy in the spectra analyses (Fig. 6), in the 1–2 day band, comes from propagating topographic waves.

Acknowledgements. This work was supported by DARDO (ENE2012-38772-C02-02), Rises-AM (GA603396), Plan-Wave (CTM2013-45141-R) and ICoast project (Echo/SUB/2013/661009). We would like to thank Joan Puigdefàbregas, Jordi Cateura and Joaquim Sospedra (LIM-UPC, Barcelona, Spain) for the data acquisition campaign. The authors thank Alexis Beudin (USGS, Woods Hole, USA) and Ken Brink (WHOI, Woods Hole, USA) for a number of useful suggestions. We are also very grateful to our reviewers, Vlado Malačič and one anonymous oceanographer, for their ideas; Vlado Malačič raised the issue of the potential relevance of coastal waves, which meant a substantial reanalysis of our velocity data and a reinterpretation of our results. Finally, we are pleased to acknowledge Gabriel Csanady and Steve Lentz, as their seminal studies on the circulation of the coastal ocean have been a source of inspiration to our work.

Edited by: S. Carniel

References

Booij, N., Ris, R. C. and Holthuijsen, L. H.: A third-generation wave model for coastal regions: 1. Model description and validation, J. Geophys. Res., 104, 7649, doi:10.1029/98JC02622, 1999.

Brink, K. H. and Chapman, D. C.: Programs for Computing Properties of Coastal Trapped waves and Wind-driven Motions over the Continental Shelf and Slope, Woods Hole Oceanographic Institute Tech. Rep. WHOI 85-17, 99 pp., 1985.

Csanady, G. T.: Circulation in the coastal ocean, Adv. Geophys., 23, 101–183, 1981.

Csanady, G. T.: Circulation in the coastal ocean, D. Reidel Publishing Company, 279 pp., Dordretch, Holland, 1982.

Dzwonkowski, B., Park, K., Lee, J., Webb, B. M., and Valle-Levinson, A.: Spatial variability of flow over a river-influenced inner shelf in coastal Alabama during spring, Cont. Shelf Res., 74, 25–34, 2014.

Fewings, M. R. and Lentz, S. J.: Momentum balances on the inner continental shelf at Martha's Vineyard Coastal Observatory, J. Geophys. Res., 115, C12023, doi:10.1029/2009JC005578, 2010.

Garvine, R. W.: The vertical structure and subtidal dynamics of the inner shelf off New Jersey, J. Mar. Res., 62, 337–371, 2004.

Gill, A. E.: Atmosphere-ocean dynamics, Academic Press, London, England, 662 pp., 1982.

Grifoll, M., Aretxabaleta, A. L., Espino, M., and Warner, J. C.: Along-shelf current variability on the Catalan inner-shelf (NW Mediterranean), J. Geophys. Res., 117, 1–14, 2012.

Grifoll, M., Aretxabaleta, A. L., Pelegrí, J. L., Espino, M., Warner, J. C., and Sánchez-Arcilla, A.: Seasonal circulation over the Catalan inner-shelf (northwest Mediterranean Sea), J. Geophys. Res. Ocean., 118, 5844–5857, 2013.

Grifoll, M., Gracia, V., Aretxabaleta, A. L., Guillén, J., Espino, M., and Warner, J. C.: Formation of fine sediment deposit from a flash flood river in the Mediterranean Sea, J. Geophys. Res. Ocean., 119, 5837–5853, 2014.

Hickey, B. M.: The Fluctuating Longshore Pressure Gradient on the Pacific Northwest Shelf: A Dynamical Analysis, J. Phys. Oceanogr., 14, 276–293, 1984.

Jordi, A., Orfila, A., Basterretxea, G., and Tintoré, J.: Coastal trapped waves in the northwestern Mediterranean, Cont. Shelf. Res., 25, 185–196, 2005.

Kirincich, A. R., Barth, J. A.: Alongshelf Variability of Inner-Shelf Circulation along the Central Oregon Coast during Summer, J. Phys. Oceanogr., 39, 1380–1398, 2009.

Kohut, J. T., Glenn, S. M., and Paduan, J. D.: Inner shelf response to Tropical Storm Floyd, J. Geophys. Res., 111, C09S91, doi:10.1029/2003JC002173, 2006.

Kundu, P. K. and Thomson, J. P.: Inertial oscillations due to a moving front, J. Phys. Oceanogr., 15, 1076–1084, 1985.

Kundu, P. K., Chao, S., and McCreary, J. P.: Transitient coastal currents and inertia-gravity waves, Deep-Sea Res., 30, 10A, 1059–1082, 1983.

Large, W. G. and Pond, S.: Open Ocean Momentum Flux Measurements in Moderate to Strong Winds, J. Phys. Oceanogr., 11, 324–336, 1981.

Lee, T. N., Ho, W. J., Kourafalou, V., and Wang, J. D.: Circulation On the Continental Shelf of the Southeastern United States, Part I: Subtidal Response to Wind and Gulf Stream Forcing During Winter, J. Phys. Oceanogr., 14, 1001–1012, 1984.

Lentz, S.: Current dynamics over the northern California inner shelf, J. Phys. Oceanogr., 24, 2461–2478, 1994.

Lentz, S., Guza, R. T., Elgar, S., Feddersen, F., and Herbers, T. H. C.: Momentum balances on the North Carolina inner shelf, J. Geophys. Res., 104, 18205–18226, 1999.

Lentz, S. J. and Fewings, M. R.: The Wind- and Wave-Driven Inner-Shelf Circulation, Ann. Rev. Mar. Sci., 4, 317–343, 2012.

Lentz, S. J. and Winant, C. D.: Subinertial Currents on the Southern Califoinia Shelf, J. Phys. Oceanogr., 16, 1737–1750, 1986.

Longuet-Higgins, M. and Stewart, R.: Radiation stresses in water waves; a physical discussion, with applications, Deep-Sea Res., 11, 529–562, 1964.

Maza, M., Voulgaris, G., and Subrahmanyam, B.: Subtidal inner shelf currents off Cartagena de Indias, Caribbean coast of Colombia, Geophys. Res. Lett., 33, 1–5, 2006.

Michaud, H., Marsaleix, P., Leredde, Y., Estournel, C., Bourrin, F., Lyard, F., Mayet, C., and Ardhuin, F.: Three-dimensional modelling of wave-induced current from the surf zone to the inner shelf, Ocean Sci., 8, 657–681, 2012.

Michaud, H., Leredde, Y., Estournel, C., Berthebaud, É., and Marsaleix, P.: Modelling and in-situ measurements of intense currents during a winter storm in the Gulf of Aigues-Mortes (NW Mediterranean Sea), Comptes Rendus Geosci., 345, 361–372, 2013.

Salat, J., Tintore, J., Font, J., Wang, D.-P., and Vieira, M.: Near-Inertial Motion on the Shelf-Slope Front off Northeast Spain, J. Geophys. Res., 97, 7277–7281, 1992.

Scott, J. T. and Csanady, G. T.: Nearshore Currents off Long Island, J. Geophys. Res., 81, 5401–5409, 1976.

Shearman, R. K.: Observations of near-inertial current variability on the New England shelf, J. Geophys. Res., 110, C02012, doi:10.1029/2004JC002341, 2005.

Tintoré, J., Wang, D.-P., García, E., and Viúdez, A.: Near-Inertial Motion in the coastal ocean, J. Mar. Syst., 6, 301–312, 1995.

Weatherly, G. and Martin, P.: On the structure and dynamics of the oceanic bottom boundary layer, J. Phys. Oceanogr., 8, 557–570, 1978.

Winant, C. D. and Beardsley, R. C.: A Comparison of Some Shallow Wind-Driven Currents, J. Phys. Oceanogr., 9, 218–220, 1979.